

Development of Semi-automatic Segmentation Methods for Measuring Tibial Cartilage Volume

James Cheong¹, David Suter¹ and Flavia Cicuttini²

¹ Department of Electrical and Computer Systems Engineering
Monash University, Clayton, Vic. 3800, Australia
{james.cheong ; d.suter}@eng.monash.edu.au

² Department of Epidemiology and Preventive Medicine
Monash University Medical School, Alfred Hospital, Prahran, Vic. 3181, Australia
flavia.cicuttini@med.monash.edu.au

Abstract

Osteoarthritis is a chronic and crippling disease affecting an increasing number of people each year. With no known cure, it is expected to reach epidemic proportions in the coming years. Currently, there is strong interest in developing a fully automated cartilage area/volume measurement method in the medical field to assist both pharmaceutical companies and medical professions in researching the disease. This paper describes the development of two different semi-automatic methods for segmenting and measuring human knee cartilage volume from magnetic resonance imaging (MRI) scans. Two different approaches were adopted, a data driven segmentation technique using directional Canny filters and a model based segmentation method using an improved Active Shape Model (ASM) scheme. The cartilage volume obtained using each method was benchmarked against the current "gold standard" (cartilage volume from manual segmentation).

1. Introduction

According to the Arthritis Foundation of Australia, over 3.4 million Australians suffer from some form of arthritis. It is estimated that 16.7% of the population have some form of arthritis at a total cost of \$11.2 billion to the community each year. Arthritis is a major public health problem and has been listed by the Australian government as one of the National Health Priority Area. Arthritis means "joint inflammation" and is a serious chronic condition with no known cure. There is currently an urgent need to better understand the disease, as arthritis is a major cause of disability and pain in Australia.

Osteoarthritis (OA) is the most common form of arthritis and involves the gradual break down and

loss of articular (joint) cartilage. It affects about 14% of the adult population [1] and is most prevalent in the knee and hip joints. Recent studies have shown that knee cartilage volume can be measured accurately and reproducibly from MRI scans [2-4]. Radiologic assessment of joint space narrowing (JSN) is currently recommended as the best measure of OA progression and studies have shown that cartilage volume measured from MRI scans correlate with the radiographic grading of OA [5-7]. Changes in cartilage volume are currently being used as a marker to predict OA onset or progression, and such measurements are emerging as a possible measure of OA severity in the knee [8].

Quantifying cartilage volume in OA will enable evaluation of therapies that may slow down or stop cartilage degradation and also preventive OA developing. There is a strong demand to automate the measurement process because large-scale clinical trials and epidemiological studies will be needed to address these issues. Research by the team of the 3rd author (Cicuttini) at the Department of Epidemiology and Preventive Medicine indicate that measurement of the tibial cartilage alone is a valid indicator of cartilage volume [9, 10]. The tibial cartilage is a clearly defined anatomical structure and thus enables measurements that are easily reproducible. Measuring and segmenting the femoral cartilage is less reproducible and more inaccurate because it is a continuous structure and forms part of three joints, the patellofemoral, lateral tibiofemoral and medial tibiofemoral joints. The femoral cartilage articulates with the patella, medial and lateral tibial cartilages and this makes it difficult to find the most appropriate component to measure.

Today, it is widely accepted that T1-weighted gradient echo sequences with spectral fat suppression displays cartilage with high contrast to surrounding tissue [11]. These sequences produce images in which the cartilage appear bright

compared to all other tissue. Images of a patient's knee are obtained using MRI with such a setup. The scans obtained are greyscale images in the sagittal plane and consists typically of 60 images (slices) for each knee. Current methods of cartilage volume measurement involve some form of manual segmentation carried out by a trained clinician. The key steps in this segmentation process involve delineating the cartilage and separating it from the surrounding tissues. Using some form of medical display software, the clinician will visually inspect and identify the presence of cartilage on each image slice. If cartilage is present, the cartilage boundary is manually traced, see Fig 1. After all 60 slices have been processed, the cartilage volume can be estimated using Cavalieri's principle [12, 13], where the sum of the segmented cartilage area is multiplied by the inter-slice distance (slice thickness).

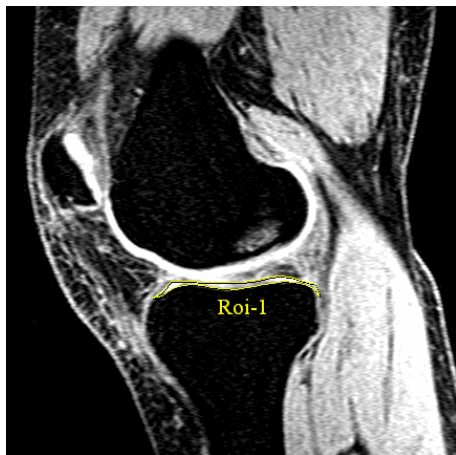


Fig 1. MRI of the knee in the sagittal plane, displaying tibial cartilage that has been manually segmented by a clinician.

This manual process is laborious and can take up to 1 hour to process a single patient knee. It is also subject to the judgement of the clinician and requires significant experience and training to obtain accurate and reproducible results. These factors increase the demand for automating the segmentation process. There are currently a number of semi-automated segmentation methods that have been developed [14-19]. These usually involve a human operator initialising the procedure by setting a number of starting points for each slice where cartilage is present, followed by an automated segmentation process. Edge detection, active contours (snakes), template matching, and statistical models are some of the segmentation techniques used. We present in this paper two different semi-automated segmentation methods for measuring tibial cartilage volume. One method is based on directional Canny filters, and the other an improved Active Shape Model (ASM) scheme.

The paper is organised as follows. In Section 2, we provide a brief description and the implementation details of the directional Canny filter segmentation method. In Section 3, ASM is described briefly, followed by a detailed description of our improved ASM segmentation method. In Section 4, we present some results of both segmentation algorithms. Discussion and concluding remarks are given in Section 5 and Section 6 respectively.

2. Direction Canny Method

2.1. Overview

This segmentation method improves on the method proposed by Lynch [16] and was written in Java as a plugin for ImageJ [20]. Each image slice is segmented individually using an edge detection algorithm based on the Canny edge detector [21]. If tibial cartilage is detected in an image, the user places 8 points close to one of the boundaries of the cartilage by clicking on the appropriate locations on the image, see Fig 2. These points form a cubic spline, where the first and the last point are called "end points" and the points in between, "control points". The end points have to be placed with a bit of precision at each end of the tibial cartilage extremity while the control points can be placed loosely around the area of the cartilage boundary. This is because only the positions of the control points are optimised to detect the cartilage boundaries. When these points are placed in satisfactory positions, the segmentation algorithm is performed and the user is presented with an outline of the tibial cartilage with an adjustable boundary. If this outline is not "correct", the user has the option of manually adjusting it.

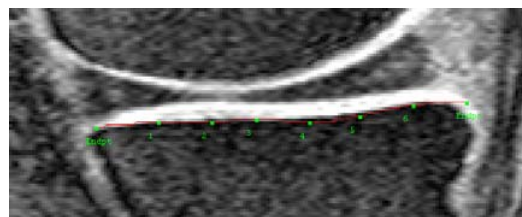


Fig 2. User places 2 end points and 6 control points.

2.1. Implementation

The segmentation process involves 2 key steps. The first step is to locate a cubic spline that runs approximately along the center of the cartilage. This is achieved by smoothing the image and locating pixels that return a high intensity value. The intuition is that cartilage regions generally have higher

intensity values compared to the surrounding bone/tissue, which have much lower intensity values. Therefore, by smoothing the image, the boundaries of the cartilage will be blurred and decrease in intensity due to the surrounding bone/tissue while the middle region of the cartilage will still contain pixels of high intensity. By locating these pixels of high intensity in the blurred image, we can locate the middle of the cartilage.

When the middle of the cartilage has been detected, the next step is to detect the boundaries of the cartilage. For the tibial cartilage, two boundaries have to be detected, the bone-cartilage interface (lower boundary) and the boundary closest to the femur (upper boundary). This second step involves driving two cubic splines in opposite directions from the middle of the cartilage, each towards one of the cartilage boundaries. This is achieved by exploiting the characteristic shape of the tibial cartilage and the intensity values of the surrounding bone/tissue structure. In a large proportion of the MRI scans, the tibial cartilage appears as a horizontal strip of cartilage of high pixel intensity, surrounded by bone/tissue of lower pixel intensity. By calculating the image gradient in the y-axis, the two boundaries of the tibial cartilage can be differentiated and located due to the opposing values of the image gradient at each boundary.

To implement the first step, the original image is smoothed from a coarse to fine scale using a Gaussian filter and optimising a cost function calculated from the filter responses, refer to (1). The purpose of this cost function is to detect the optimal positions for the control points of the center spline. Firstly, 5 evenly distributed points are inserted between each of the 8 points placed by the user, and the Gaussian filter response at each of these 43 points is summed. Because the length of the tibial cartilage is not large, placing more than 5 points between each point might result in repeated points. The cost function is then iteratively minimised by altering the position of the control points and recalculating the effect on the cost function. The positions of the end points are fixed, thus only the positions of the control points are moved. The 4 possible positions for the control point being adjusted are inward and outward perpendicular to the local spline direction, and in the two directions parallel to the local tangent to the spline. When the cost function cannot be reduced any further, the process stops. This optimisation process is run twice, the first time using a coarse scale Gaussian filter ($\sigma = 2$) and adjusting the control points by 2 pixels; and the second time using a finer scale Gaussian filter ($\sigma = 1$) and adjusting the control points by 1 pixel.

$$\text{cost} = \frac{-\sum_{i=1}^{43} \text{Filter Response}}{A \times (\text{Resultant Spline Length})} \quad (1)$$

To implement the second step, an optimisation algorithm similar to that previously described is used. Instead of Gaussian filters, directionally oriented Canny filters are used. The “normal” Canny edge detector [21] finds edges by looking for local maxima of the image gradient. In the case of directional Canny edge detection, the filter response $R(\Theta)$ is defined as:

$$R(\Theta) = R_x \cos \Theta + R_y \sin \Theta, \quad (2)$$

where R_x = image gradient in the x direction and R_y = image gradient in the y direction. Edges at the specified angle Θ return a positive filter response, while edges at $(\Theta+180^\circ)$ return a negative filter response. See Fig 3, where grey areas represent a value close to zero, white areas represent strong positive values and black areas, strong negative values. NOTE: With the origin of the image at the top left corner, $\Theta = 0^\circ$ is horizontal with increasing x and $\Theta = 90^\circ$ is vertical with increasing y. We set $\Theta = 90^\circ$, thus eliminating the response in the horizontal x axis and including only the vertical response of the y axis. This enables the detection of the lower and upper boundaries of the cartilage from the sign of the filter response because when $\Theta = 90^\circ$, the response of the directional Canny filter returns values that are opposite in sign on either side of the tibial cartilage boundary, see Fig 3.

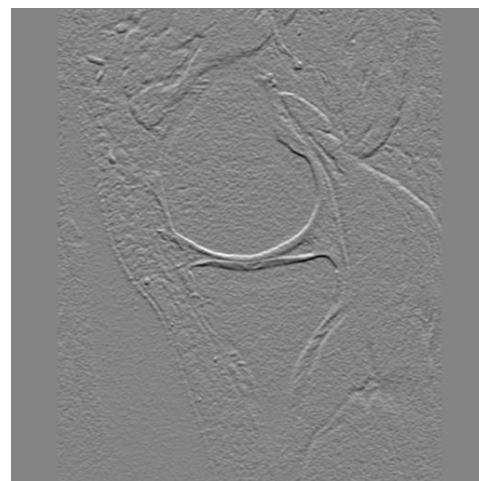


Fig 3. Directional Canny response with $\Theta=90^\circ$

The cost function for the second optimisation algorithm is the same as that used to detect the center spline. 5 evenly distributed points are inserted once

again between the 8 points that define each spline. The directional Canny filter response with Θ set to 90° is calculated and the response for each of the 43 points are summed and divided by the length of the resulting spline. To detect the lower boundary, the filter response is multiplied by -1 , while for the upper boundary, the filter response is left as it is. Similarly, the cost function is iteratively optimised for the lower and upper boundaries by altering the position of the control points. When the cost function cannot be reduced any further or when an upper limit for the number of iterations is reached, the process stops. The upper limit minimises the deviation of the spline from the actual cartilage boundary and must be large enough so that it does not stop the optimisation prematurely. The optimisation algorithm is run twice, the first time using a coarse scale ($\sigma = 2$) to calculate the image gradient and the second time using a finer scale ($\sigma = 1$). The control points are adjusted by 1 pixel for both cases.

3. Improved ASM Method

3.1. Active Shape Models (ASM)

ASM [22] represents objects as a set of n labelled points referred to as landmarks. These landmarks are extracted from a set of s training images either manually or automatically. A point distribution model (PDM) is then constructed to model the variation distribution of the landmarks as follows. The landmarks $(x_1, y_1, \dots, x_n, y_n)$ for each training image are stacked into a shape vector, \mathbf{x}_i ,

$$\mathbf{x}_i = (x_1, y_1, \dots, x_n, y_n)^T \quad (3)$$

The shape vectors are aligned by scaling, rotation and translation using an iterative scheme known as Procrustes analysis [23]. Alignment is done to minimise the sum of squared distance between the landmarks. A mean shape is then calculated from the shape vectors \mathbf{x}

$$\bar{\mathbf{x}} = \frac{1}{s} \sum_{i=1}^s \mathbf{x}_i \quad (4)$$

as well as the covariance matrix

$$\mathbf{S} = \frac{1}{s-1} \sum_{i=1}^s (\mathbf{x}_i - \bar{\mathbf{x}})(\mathbf{x}_i - \bar{\mathbf{x}})^T. \quad (5)$$

Principal component analysis (PCA) is then applied using eigenvalue decomposition of the covariance matrix. Eigenvectors corresponding to the t largest eigenvalues λ_i are retained in a matrix \mathbf{P} . The

number of eigenvalues to retain, t , is chosen such that their sum sufficiently explains the variance in the training shapes, since the variance explained by each eigenvector is equal to the corresponding eigenvalue. t is usually chosen such that the explained variance ranges from 90% to 99.5% of the sum of all the eigenvalues. Any shape in the training set can now be approximated by

$$\mathbf{x} = \bar{\mathbf{x}} + \mathbf{P}\mathbf{b}, \quad (6)$$

where \mathbf{b} is a vector of t elements containing the model parameters, calculated by

$$\mathbf{b} = \mathbf{P}^T(\mathbf{x} - \bar{\mathbf{x}}). \quad (7)$$

To ensure that new shapes generated are in the allowable shape domain, the values of \mathbf{b} are constrained to lie within the range $\pm \mathbf{m}\sqrt{\lambda_i}$, where \mathbf{m} has a value between two and three.

3.2. Image Gradient Appearance Model

Each image in the training set is filtered with the vertical 3×3 Sobel operator.

$$\begin{bmatrix} 1 & 2 & 1 \\ 0 & 0 & 0 \\ -1 & -2 & -1 \end{bmatrix} \quad (8)$$

A $\mathbf{k} \times \mathbf{k}$ matrix profile of the resulting image gradient is then collected for each landmark. When all images in the training set have been processed, a mean image gradient matrix profile is calculated for each landmark. The intuition behind this step is that the image gradient contains useful edge information for segmenting tibial cartilage, as evidenced by the directional Canny method.

3.3. Training and Implementation

Landmarks for our training set were obtained automatically using a Minimum Description Length (MDL) shape algorithm developed by Thodberg [24]. The algorithm seeks a user defined number of landmarks from a set of shapes. From our database of over 1500 tibial cartilage manually segmented by clinicians, we obtained 32 landmarks for each of the corresponding MRI image.

This segmentation method was implemented in MATLAB and shows better segmentation results for tibial cartilage than the original ASM method by Cootes [22, 25]. If tibial cartilage is detected in an image, the user places 2 end points on the cartilage and the segmentation algorithm is performed.

Cartilage segmentation basically involves iteratively searching an image for an allowable shape

given an initial estimate of the end points of the cartilage. An initial estimate is created by fitting a scaled and translated version of the mean shape between the user placed end points. The neighbourhood of each landmark of the estimate is then examined to find better locations for the landmarks. This is implemented by filtering the image being searched with the vertical 3x3 Sobel operator, and examining a 3kx3k profile of the image gradient around each landmark. The kxk region in the search profile that returns the smallest error when compared with the mean image gradient model is the new location of the landmark.

The shape and pose of the estimate is then updated, constrained by limits set to the variation of **b**, so that the new shape is within the allowable shape domain. This procedure is iterated until it converges, i.e. there is no significant change in shape between two consecutive iterations. The result is a set of points $\hat{x} = (x_1, y_1, \dots, x_n, y_n)^T$ being an estimation of the tibial cartilage in the image.

4. Results

Experiments were performed to determine the segmentation and measurement accuracy of both methods. Both segmentation accuracy and measurement accuracy were determined by comparing the cartilage area collected from our method with those derived by the manual method. The difference between segmentation and measurement accuracy is that for segmentation accuracy, the user does not manually adjust the detected boundaries if they do not “correctly” outline the cartilage. With measurement accuracy, the user has the option of adjusting the boundaries before recording the area measurements. Fig 4 shows the outline of a tibial cartilage manually segmented by a clinician. Fig 5, Fig 6 and Fig 7 show the segmentation results for our directional Canny method, the improved ASM method, and Cootes’ original ASM method respectively on the same cartilage slice.

Fig 8 compares the cartilage area measured using the manual method and the semi-automatic methods from a patient knee. This figure shows that the manual and semi-automatic measurement methods measure the same pattern of cartilage area within the joint. The ASM methods fail to correctly segment tibial cartilage in the middle of the knee, therefore data in that region could not be obtained. To examine the relationship between the measurements, a regression between the paired measurements from the semi-automatic methods and the manual method was performed, see Fig 9 to Fig 12.

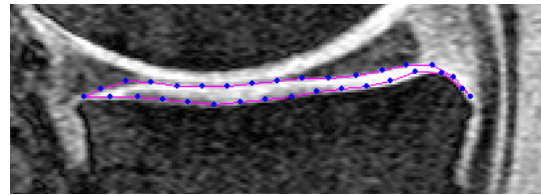


Fig 4. Manually segmented tibial cartilage

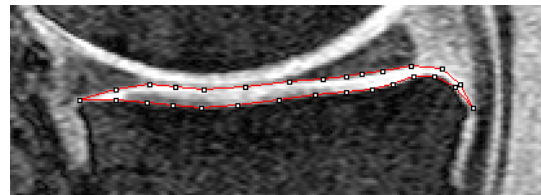


Fig 5. Segmentation using d-Canny method without manual adjustments

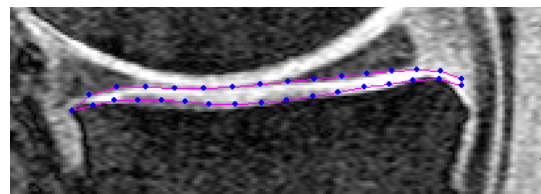


Fig 6. Segmentation using improved ASM method

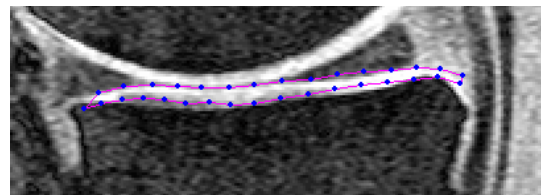


Fig 7. Segmentation using original ASM method

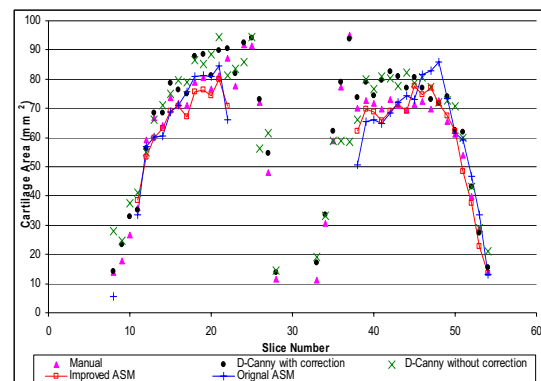


Fig 8. Comparison of manual and semi-automated measurements for a patient. Image sequence is from medial (lower slice numbers) to lateral (higher slice numbers)

The linear regression line in Fig 9 shows strong correlation between the measurements of the manual and the directional Canny segmentation method

when the user can manually correct the boundaries. If the boundaries were not adjusted, the linear regression line still shows a good correlation between the measurements, see Fig 10. However, this correlation is not as strong as when the boundaries are manually adjusted. The linear regression in Fig 11 shows a strong correlation between the manual measurements and the improved ASM method, even though the boundaries are not manually adjusted. This correlation is stronger compared to that between the manual measurements and Coote's original ASM method in Fig 12.

The results obtained correspond well with those measured using the manual method. In addition, we found that the semi-automatic methods of segmentation could be easily learnt by other users and can reduce the time taken to process a single patient knee. Initial testing indicated less than 20 min to process a patient, compared to 60 min using the manual method. These figures are rough estimates and more precise data have to be collected to validate them. The users were also in the process of learning the operation of the system when these timings were taken. With more familiarity, we expect the time taken to be even shorter.

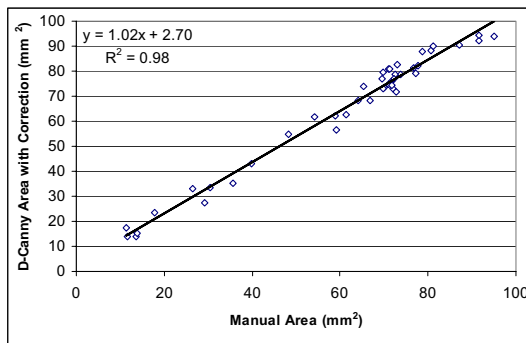


Fig 9. Relationship between areas measured from manual and D-Canny method.

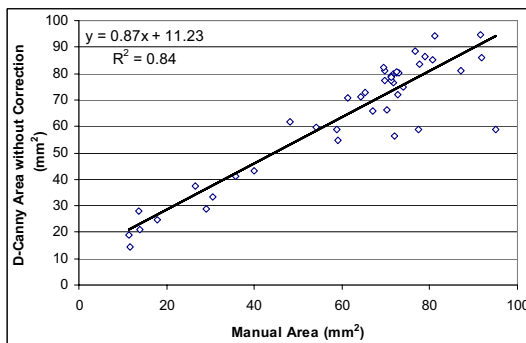


Fig 10. Relationship between areas segmented from manual and D-Canny method. Boundaries from D-Canny method have not been adjusted by user.

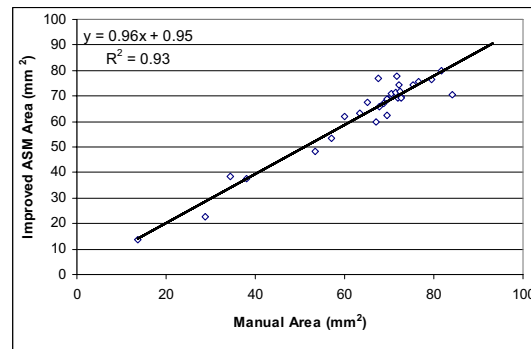


Fig 11. Relationship between areas segmented from manual and improved ASM method.

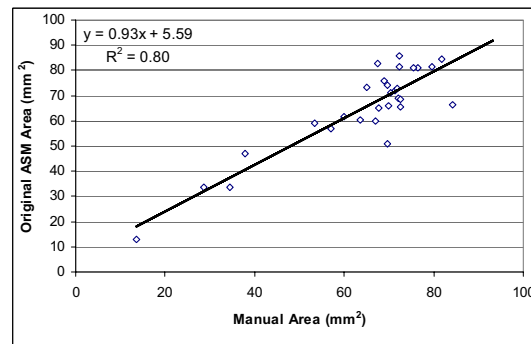


Fig 12. Relationship between areas segmented from manual and original ASM method.

5. Discussion

Our data have shown that the semi-automatic methods display a high degree of measurement and segmentation accuracy. The other segmentation techniques mentioned in Section I focus on segmenting the femoral cartilage and only present results from a small number of patients, or in some cases, only a few MRI slices. This makes it difficult to compare their results with our own.

Cootes [22, 25] proposed a grey-level appearance model where the greyscale pixel profile around each landmark is obtained. A normalised derivative profile is obtained so that the profile is invariant to the offsets and uniform scaling of the grey levels. The results show that the grey-level appearance model does not measure tibial cartilage area as well as our image gradient appearance model. This is because in some images, the range of pixel intensities that define a cartilage region can be very large due to the biochemically heterogeneous property of cartilage. A model that profiles image gradient provides more useful edge information for segmenting the cartilage boundary, compared with just the greyscale pixel intensities.

In general, the segmentation using the directional Canny method works well and little or no adjustments are required to correct the outline. The number of slices where incorrect segmentation occurs for a patient knee is highly dependent on the set up of the MRI scanner. In MRI, the tissue contrast can be adjusted by selecting different types of pulse sequences and by changing the parameters of these sequences such as repetition time, echo time, flip angle, etc. Even though it is widely accepted that T1-weighted gradient echo sequences with spectral fat suppression visualises cartilage with high contrast to surrounding tissue, there is no agreed setting for repetition time, echo time and flip angle. This leads to MRI images with varying tissue contrast between patients and this is a common problem encountered by data driven segmentation methods such as the directional Canny method.

A common problem encountered with segmenting cartilage occurs when processing images where the femoral and tibial cartilages are in contact, see Fig 13. Because some parts of the cartilage are actually in contact, there is no edge information for the upper boundary of the tibial cartilage. This causes the directional Canny method to steer towards the bone-cartilage boundary of the femoral cartilage instead. This problem is overcome by adopting a model based segmentation technique. Our ASM method restricts shape deviation by locking onto landmarks in the image with strong resemblance to the image gradient model and interpolating the expected positions of the other landmarks with weaker resemblance to the model. This overcomes the problem of some missing edge information but still producing an allowable shape, see Fig 14. The improved ASM method also requires less user interaction compared to the directional Canny method. Users are only required to identify 2 end points with the ASM method, compared with 2 end points and 6 control points using the directional Canny method.

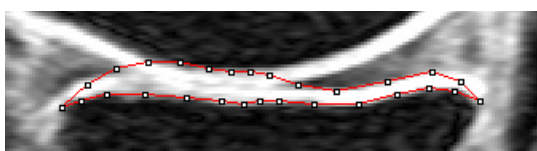


Fig 13. Segmentation using D-Canny method due to cartilage touching

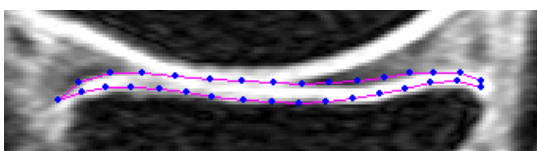


Fig 14. Segmentation using improved ASM method on the same cartilage slice

However, our ASM method has its disadvantages too. This method fails to segment cartilage in the middle region of the knee, where the cartilage shape is highly variable. We tried training the method on a set of cartilage shapes derived from the middle region of the knee, but the results were not good. The large shape variation in that region also affects the directional Canny method because a large proportion of the cartilage boundary in that region have to be manually adjusted.

6. Conclusion and Further Work

We have developed two segmentation methods for tibial cartilage. Both segmentation methods have been tested and compared with the current "gold" standard of manual measurements and have displayed a high degree of measurement and segmentation accuracy. Both methods have their pros and cons and we intend to exploit the advantages of each method to develop a semi-automatic system for quantitating knee cartilage volume.

To date we have only examined our segmentation method on healthy knees. We intend to test the segmentation method on MRI images of osteoarthritic knee, where cartilage edges may be less well defined.

References

- [1] M. D. Forman, R. Malamet, and D. Kaplan, "A survey of osteoarthritis of the knee in the elderly," *The Journal of Rheumatology*, vol. 10, pp. 282-287, 1983.
- [2] F. Eckstein, J. Westhoff, H. Sittek, K.-P. Maag, M. Haubner, S. Faber, Englemeier K.-H., and M. Reiser, "In vivo reproducibility of three-dimensional cartilage volume and thickness measurements with MR imaging," *American Journal of Roentgenology*, vol. 170, pp. 593-597, 1998.
- [3] F. Cicuttini, A. Forbes, K. Morris, S. Darling, M. Bailey, and S. Stuckey, "Gender differences in knee cartilage volume as measured by magnetic resonance imaging," *Osteoarthritis and Cartilage*, vol. 7, pp. 265-271, 1999.
- [4] G. Jones, M. Glisson, K. Hynes, and F. Cicuttini, "Sex and site differences in cartilage development: a possible explanation for variations in knee osteoarthritis in later life," *Arthritis & Rheumatism*, vol. 43, pp. 2543-2549, 2000.
- [5] M. Glisson, A. Forbes, K. Morris, S. Stuckey, and F. Cicuttini, "Comparison of

- x-rays and magnetic resonance imaging in the definition of tibiofemoral joint osteoarthritis," *Radiography*, vol. 6, pp. 205-209, 2000.
- [6] F. Eckstein, F. Cicuttini, J. P. Raynauld, J. C. Waterton, and C. Peterfy, "MRI of articular cartilage in knee osteoarthritis: morphological assessment," unpublished.
- [7] F. Cicuttini, A. E. Wluka, A. Forbes, and R. Wolfe, "Comparison of tibial cartilage volume and radiologic grade of the tibiofemoral joint," *Arthritis & Rheumatism*, vol. 48, pp. 682-688, 2003.
- [8] J. P. Raynauld, "Magnetic resonance imaging of articular cartilage: toward a redefinition of "primary" knee osteoarthritis and its progression," *The Journal of Rheumatology*, vol. 29, pp. 1809-1810, 2002.
- [9] F. Cicuttini, A. E. Wluka, and S. L. Stuckey, "Tibial and femoral cartilage changes in knee osteoarthritis," *Annals of the Rheumatic Diseases*, vol. 60, pp. 977-980, 2001.
- [10] F. Cicuttini, A. E. Wluka, Y. Wang, and S. L. Stuckey, "Longitudinal study of changes in tibial and femoral cartilage in knee osteoarthritis," *Arthritis & Rheumatism*, vol. 50, pp. 5-9, 2004.
- [11] M. P. Recht, J. Kramer, S. Marcelis, M. N. Pathria, D. Trudell, P. Haghghi, D. J. Sartoris, and D. Resnick, "Abnormalities of articular cartilage in the knee: analysis of available MR techniques," *Radiology*, vol. 187, pp. 473-478, 1993.
- [12] B. Caverlieri, *Geometria Indivisibilibus Continuorum*: Bononi: Typis Clemetis Feronij, 1635. Reprinted as *Geometria degli Indivisibili*. Torino: Unione Tipografico-Editorice Torinese, 1966.
- [13] N. Roberts, "Unbiased estimations of volume: some notes for ANALYZE™ users," in *Biomedical Imaging Resource, ANALYZE Reference Manual. Revision 7.5*. Rochester, Minnesota: Mayo Foundation, 1996, pp. III 302-307.
- [14] Z. A. Cohen, D. M. McCarthy, S. D. Kwak, P. Legrand, F. Fogarasi, E. J. Ciaccio, and G. A. Ateshian, "Knee cartilage topography, thickness, and contact areas from MRI: in-vitro calibration and in-vivo measurements," *Osteoarthritis and Cartilage*, vol. 7, pp. 95-109, 1999.
- [15] A. A. Kshirsagar, P. J. Watson, J. A. Tyler, and L. D. Hall, "Quantitation of articular cartilage dimensions by computer analysis of 3D MR images of human knee joints," *Proceedings of the 19th Annual International Conference of the IEEE Engineering in Medicine and Biology Society*, vol. 19, pp. 753-756, 1997.
- [16] J. A. Lynch, S. Zaim, J. Zhao, A. Stork, C. G. Peterfy, and H. K. Genant, "Cartilage segmentation of 3D MRI scans of the osteoarthritic knee combining user knowledge and active contours," *Proceedings of SPIE*, vol. 3979, pp. 925-935, 2000.
- [17] T. Stammberger, F. Eckstein, M. Michaelis, K.-H. Englmeier, and M. Reiser, "Interobserver reproducibility of quantitative cartilage measurements: comparison of B-spline snakes and manual segmentation," *Magnetic Resonance Imaging*, vol. 17, pp. 1033-1042, 1999.
- [18] S. K. Warfield, M. Kaus, F. A. Jolesz, and R. Kikinis, "Adaptive, template moderated, spatially varying statistical classification," *Medical Image Analysis*, vol. 4, pp. 43-55, 2000.
- [19] S. Solloway, C. J. Taylor, C. E. Hutchinson, and J. C. Waterton, "Quantification of articular cartilage from MR images using active shape models," *Proceedings of the 4th European Conference on Computer Vision*, vol. 2, pp. 400-411, 1996.
- [20] W. S. Rasband, "ImageJ." National Institutes of Health, Bethesda, Maryland, USA: <http://rsb.info.nih.gov/ij/>, 1997-2005.
- [21] J. Canny, "A computational approach to edge detection," *IEEE Transactions on Pattern Analysis and Machine Intelligence*, vol. 8, pp. 679-698, 1986.
- [22] T. F. Cootes, C. J. Taylor, D. Cooper, and J. Graham, "Active shape models - their training and application," *Computer Vision and Image Understanding*, vol. 61, 1995.
- [23] C. Goodall, "Procrustes methods in the statistical analysis of shapes," *Journal of the Royal Statistical Society*, vol. 53, pp. 285-339, 1991.
- [24] H. H. Thodberg, "Minimum Description Length Shape and Appearance Models," *Proceedings of Information Processing in Medical Imaging*, pp. 51-62, 2003.
- [25] T. F. Cootes, A. Hill, C. J. Taylor, and J. Haslam, "Use of active shape models for locating structures in medical images," *Image and Vision Computing*, vol. 12, pp. 355-366, 1994.